Heliyon 10 (2024) e39892

Contents lists available at ScienceDirect

Heliyon

journal homepage: www.cell.com/heliyon

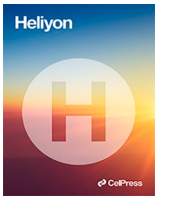

Research article

Magnoflorine ameliorates hepatic fibrosis and hepatic stellate cell activation by regulating ferroptosis signaling pathway

Meiling Zhang [a], Lenan Xu [a], Chengkai Zhu [a], Yawen Zhang [a], Ruixiang Luo [a], Juan Ren [c], Jie Yu [c], Yanmei Zhang [c], Guang Liang [a,b,**], Yi Zhang [a,*]

[a] School of Pharmaceutical Sciences, Hangzhou Medical College, Hangzhou, Zhejiang, 310012, China
[b] Chemical Biology Research Center, School of Pharmaceutical Sciences, Wenzhou Medical University, Wenzhou, Zhejiang, 325035, China
[c] School of Laboratory Medicine and Bioengineering, Hangzhou Medical College, Hangzhou, Zhejiang, 310012, China

ARTICLE INFO

Keywords:
Hepatic fibrosis
Magnoflorine
Hepatic stellate cells
Ferroptosis
Deferoxamine

ABSTRACT

Liver fibrosis is a chronic liver disease that brings a heavy economic burden to the world and has attracted global attention. Although the pathological mechanisms and treatment strategies of liver fibrosis have been extensively studied, there are currently no effective targeted drugs for the prevention and treatment of liver fibrosis in clinical practice. Therefore, it is imperative to seek and develop effective treatment strategies and drugs for liver fibrosis. Magnoflorine (MAG) is a natural product with multiple pharmacological activities. Thus, in this study, we will explore the effect of MAG on alleviating liver fibrosis in mice and its mechanism of action. Our study indicates that MAG can alleviate liver damage, improve liver collagen deposition, and significantly reduced the expression levels of hepatic stellate cells (HSCs) activation markers in vivo. Additionally, the findings of this study indicate that MAG can inhibit the transforming growth factor-beta (TGF-β)/Smad signaling pathway. Bioinformatics analysis suggests that the alleviating effect of MAG on liver fibrosis may be associated with ferroptosis. Interestingly, in vitro experiments have demonstrated that MAG slows down the progression of liver fibrosis by inhibiting the activation of HSCs, and further confirms that MAG promotes ferroptosis in ROS-mediated activated HSCs. In short, MAG has a good alleviating effect on liver fibrosis and will be a potential candidate drug for the treatment of liver fibrosis.

1. Introduction

Hepatic fibrosis (HF) is an injury repair response of the body to chronic hepatic injury of various etiologies; it manifests by the proliferation and deposition of connective tissue in the liver. Hepatic fibrosis can gradually evolve into hepatic cirrhosis and even hepatic cancer [1]. Cirrhosis, viral hepatitis, and liver cancer account for over 2 million deaths, representing 4 % of the global total deaths (i.e. 1 out of every 25 deaths). According to the aforementioned statistics, liver cancer claims between 600,000 and 900,000 lives annually. Currently, liver disease ranks as the 11th leading cause of death globally, yet the actual number of deaths attributed to liver disease may be underestimated [2]. Currently, there are no effective drugs for the treatment of hepatic fibrosis. Finding an effective treatment for the disease will bring about significant social and economic benefits.

* Corresponding author. School of Pharmaceutical Sciences, Hangzhou Medical College, Hangzhou, 310012, China.
** Corresponding author. School of Pharmaceutical Sciences, Hangzhou Medical College, Hangzhou, 310012, China.
E-mail addresses: wzmcliangguang@163.com (G. Liang), 1020437493@qq.com (Y. Zhang).

https://doi.org/10.1016/j.heliyon.2024.e39892
Received 30 July 2024; Received in revised form 25 October 2024; Accepted 25 October 2024
Available online 8 November 2024

The physiopathology of hepatic fibrosis involves various cells, cytokines and changes in the extracellular matrix (ECM). Several factors interact and influence each other, resulting in the formation of a dynamic hepatic fibrotic network. HSC are the core of this interlaced association network [3], and undergo differentiation from quiescent HSCs to myofibroblasts in disease states. Thus, the

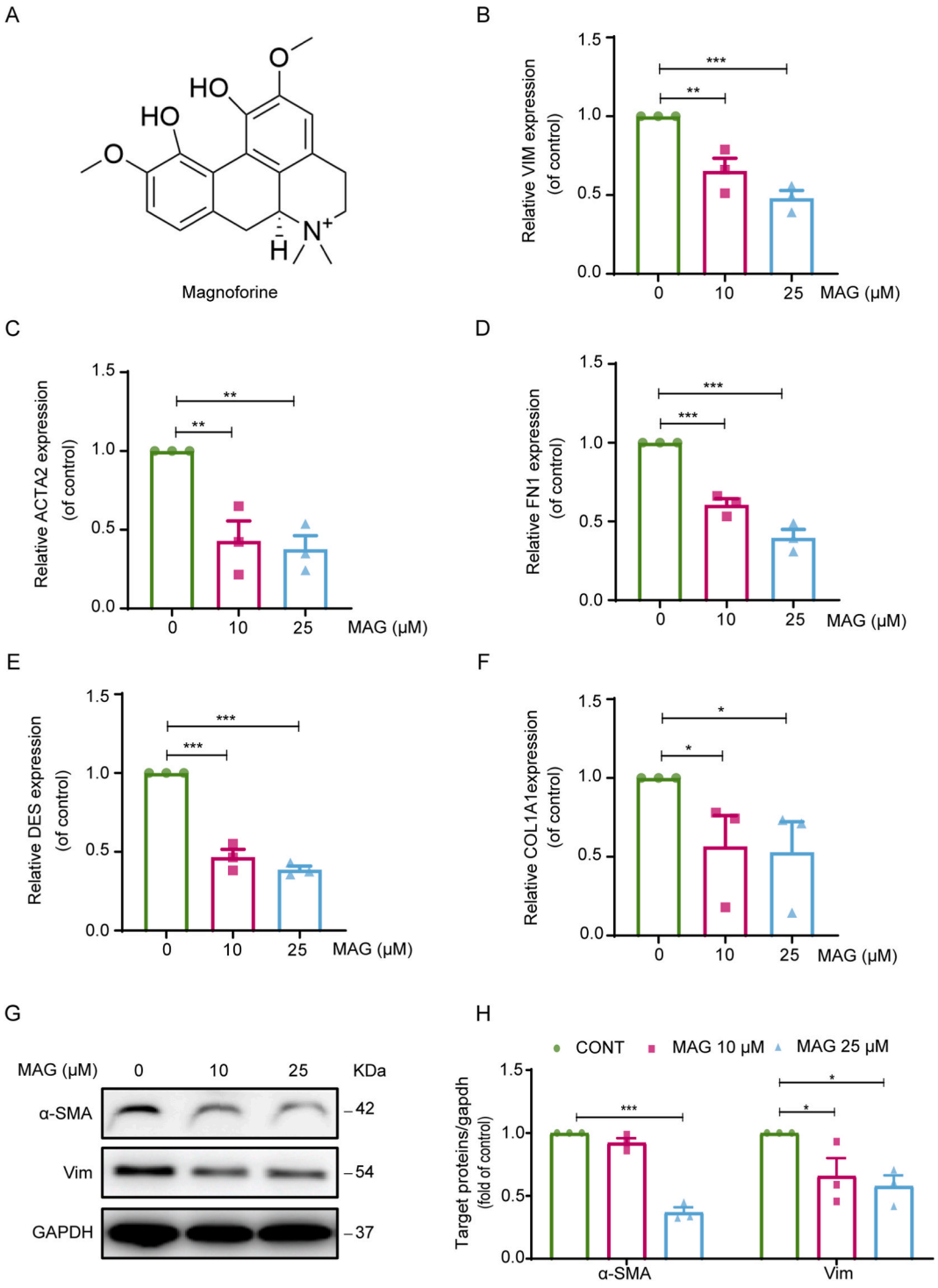

Fig. 1. MAG inhibits HSC activation in vitro. (A) The structural formula of magnoflorine. (B–F) LX-2 cell COL1A1, ACTA2 (α-SMA), VIM, FN1 DES mRNA expression (n = 3). (G) Western blot detection of α-SMA and Vim protein expression in LX-2 cells with GAPDH as a control. (H) The Statistical results of α-SMA and Vim. The results represent three independent experiments. Data were showed as means ± SEM. *$P < 0.05$; **$P < 0.01$; ***$P < 0.001$.

inhibition of HSC activation could be an effective strategy for the prevention and treatment of hepatic fibrosis. Studies have demonstrated that the inhibition of HSC proliferation and the induction of their senescence, autophagy [4], pyroptosis [5], and apoptosis [6] are potential strategies for alleviating hepatic fibrosis.

Ferroptosis is a regulated form of programmed cell death triggered by uncontrolled accumulation of iron-dependent membrane lipid peroxidation (LPO) [7]. Multiple studies indicate that disturbances in iron metabolism can trigger the formation of lipid peroxides, a process referred to as the Fenton reaction [8]. Additionally, the blockade of the cysteine/glutamate reverse transport system results in the depletion of glutathione (GSH). The suppression of glutathione peroxidase 4 (GPX4) activates substantial ROS production and the Fenton reaction within cells, causing membrane damage and ultimately triggering ferroptosis [9]. It is worth noting that ferroptosis is closely associated with the onset and progression of various liver diseases, including steatohepatitis, liver fibrosis, and liver cancer [10]. Numerous studies have shown that HSCs store a large amount of iron ions, and ferroptosis can influence the progression of liver fibrosis by regulating the iron ion content and the degree of lipid peroxidation in HSCs [11–13]. Tripartite motif-containing protein 26 (TRIM26) induces ferroptosis in HSCs by regulating the ubiquitination of solute carrier family-7 member-11 (SLC7A11), thereby mitigating the progression of liver fibrosis [14]. Moreover, studies have revealed that numerous traditional Chinese medicines can treat liver fibrosis by inducing ferroptosis in HSCs [15,16].

Alkaloids, a vital class of natural products found in plant-based medicines, exhibit significant biological activities. Magnoflorine (MAG Fig. 1A), alternatively referred to as tangsongcao alkaloid, magnolianine, stands as a classic example of an apophylline alkaloid [17]. The pharmacological activities of MAG have been extensively investigated. In recent years, increasing evidence has indicated that MAG is a promising drug candidate for the treatment of diabetes, inflammatory diseases, and neurological diseases, such as depression and Alzheimer's disease [18]. However, studies on its effects in the treatment of hepatic fibrosis are lacking. In this study, we explored the role of MAG on hepatic fibrosis and elucidated the mechanisms in which MAG alleviated ferroptosis in HSCs.

2. Materials and methods

2.1. Reagents and materials

The MAG and Silymarin (SIL) were bought from Bio-Technology Co., Ltd (Shanghai, China). Deferoxamine (DFO) was from Sigma-Aldrich (St. Louis, MO, USA). The CCK-8 was from APE × BIO Technology LLC (Houston, TX, USA). A calcein AM kit measuring for the chelatable iron pool in LX-2 cells was from Beyotime (Shanghai, China). The kits for GSH content, hydroxyproline content, ALT/AST activity were from Nanjing Jiancheng Bioengineering Institute (Nanjing, China). Antibodies against vimentin, α-SMA, desmin, TGF-β, p-Smad 2/3, Smad 2/3, SLC7A11, GPX4, SLC40A1 and GAPDH were from Cell Signaling Technology (Danvers, MA, USA).

2.2. Experimental animals

C57BL/6J male mice weighing between 18 and 22 g were provided by Hangzhou Medical College Laboratory Animal Centre (Hangzhou, China). All animal experiments were approved by the Experimental Animal Ethical Committee of Zhejiang Experimental Animal Center. The mice were raised under specific pathogen-free (SPF) conditions and randomly allocated to six groups, each consisting of seven mice: the vehicle control; CCl_4 model; CCl_4+MAG (20 mg/kg); CCl_4+MAG (40 mg/kg); MAG (40 mg/kg); CCl_4+SIL (0.2 g/kg). Subsequently, mice were treated for 2 weeks with CCl_4 (intraperitoneal injection, mixed with olive oil in the ratio 1:3,2 mL/kg twice per week) and then for an additional 4 weeks with both CCl_4 (twice per week), MAG or SIL (intragastric administration, every day). After treatment, the mice were anesthetized using phenobarbital sodium (40 mg/kg, intraperitoneal injection), and their plasma and liver tissue samples were collected.

2.3. AST/ALT activity

Determination of AST and ALT in serum was performed according to illustrative (Nanjing Jiancheng Bioengineering Institute, Nanjing, China) guidelines.

2.4. Histological evaluation of the liver

After fixing liver sample in 4 % paraformaldehyde for 24 h, a slicer was used to slice it into 4 μm thick sections. Then, the sections were placed in xylene, anhydrous ethanol, and 75 % ethyl acetate. Subsequently, the sample was deparaffinized in alcohol and rinsed with tap water. The sections were individually stained. After staining with Sirius Red, Masson trichrome, and hematoxylin-eosin (H&E) were placed in anhydrous ethanol. Then, they were immersed in xylene to make them transparent and the pathological features of the tissue were examined under an optical microscope.

2.5. Liver hydroxyproline activity

The determination of hydroxyproline content in the liver was performed according to illustrative (Nanjing Jiancheng Bioengineering Institute, Nanjing, China) guidelines.

2.6. ELISA analysis

Laminin (LN) serum content was detected using ELISA kits (RapidBio, West Hills, CA).

2.7. α-SMA immunofluorescence staining

To minimize non-specific binding, formalin-fixed and graphitized liver sections (5 μm) were incubated with 5 % BSA for 1 h. Liver sections were then incubated with anti-α-SMA antibody overnight at 4 °C. The nuclear structure of liver biopsy tissue was reacted with DAPI for 10 min and then washed three times. After that, pictures were captured with a stereomicroscope (IX81, Olympus, Japan).

2.8. Immunohistochemical staining

The specific antigen were sequentially applied in liver sections with drops of 3 % hydrogen peroxide and 5 % bovine serum albumin (BSA) for 1 h. Following blocking, a diluted waveform antibody solution was prepared according to the provided instructions and incubated overnight at 4 °C. Then, incubated with secondary antibody (Goat Anti-Rabbit IgG (H + L) HRP) at room temperature for 1 h. After the primary antibody incubates, the two-resistant incubation will be incubated at room temperature for an hour. Primary antibodies were prepared using DAB chromogenic solution, and hematoxylin was used as a counterstain for the nuclei. The parts were thoroughly cleaned, then dehydrated and cleaned again. The sections were then immersed in water until clear and then mounted and examined for pathology using light microscopy.

2.9. Cell cultivation

Hepatic stellate cell line LX-2 (ZQ0026; For Research Use Only) was derived from Qiao Xin Zhou Biotechnology Co.,Ltd. (Shanghai, China) and was maintained in high-glucose Dulbecco's Modified Eagle Medium (Bio-Channel; BC-M-005) with 10 % FBS(Bio-Channel; BC-SE-FBS08), plus 1 % penicillin/streptomycin (Biosharp; BL505A).

2.10. CCK-8 analysis

MAG was dissolved in DMSO for LX-2 administration.6×10^3 cells were seeded in 96-well plates and then incubated with different concentrations of MAG. The cell count Kit-8 (APE × Bio Technology LLC, Houston, Texas, USA) was used to evaluate cell vitality.

2.11. Cell death test

Evaluation of LX-2 cell death following MAG administration was conducted using an FDA-approved staining kit (AAT Bioquest, Sunnyvale, California, USA), with imaging analysis performed using a laser confocal instrument.

2.12. Measurement of GSH levels

After 24 h post MAG or DFO treatment, GSH levels were measured in cells using a glutathione assay kit (Nanjing Jiancheng Institute of Biotechnology, Nanjing, China).

2.13. ROS measurements

The intracellular ROS levels in LX-2 cells post-MAG administration were assessed using the oxidation-sensitive fluorescent probe DCFH-DA (Solarbio, Beijing, China), with imaging analysis conducted via laser confocal microscopy.

2.14. Mitochondrion assay

Mitochondria in cells were dyed by the MitoLite™ Red FX600 kit (AAT Bioquest, USA). The LX-2 cell density of 1 x 10^5 cells per hole was spread in six orifices and treated with DMSO (0.025 %, v/v) and MAG (10,25 μM) for 48 h. PBS-washed plates were washed four times. Cells were then dyed with Mitolite Red FX600, a 1:500 dilution of live cell staining buffer, for 60 min at 37 °C. DAPI staining the nucleus for half an hour. PBS-washed plates were washed four times; the cells were seen under an inverted luminescence microscope (EVOS M7000, USA) as above.

2.15. Iron measurements

Iron levels in LX-2 cells were Measured by the FerroOrange (Goryo Chemical Inc., Hokkaido, Japan).

2.16. RNA extraction and RT-qPCR analysis

Total RNA was isolated by RNA extraction Assisted regent and cDNA were generated by Evo M-MLV RTase following the specific

procedures. Use SYBR master mix primers and samples to perform RT-qPCR analysis according to the set procedure. The relevant reagents are from Ecorui Bioengineering Co., LTD (Hu nan,China). The analysis of the target gene was normalized to that of actin and analyzed by the $2^{-\Delta\Delta Ct}$ method, with the results expressed as a ratio to the vector control. Table S1 details the use of all primers.

2.17. Western blot

The lysis of liver and cellular proteins was achieved through the utilization of RIPA lysate (cat# P0013B; Beyotime Biological Technology, Shanghai, China), which was subsequently left on ice for a period of 10 min. Thereafter, Centrifugation at 4 °C and 10,000×*g* for 10 min. The amount of protein was normalized, with the sample exhibiting the lowest protein concentration being selected for further analysis. After the samples were uniformly quantified, an equal volume of 2x loading was added to denature the proteins at 100 °C for 10 min. Subsequently, the proteins were separated by SDS-PAGE electrophoresis and transferred to a PVDF membrane. After sealing, incubate the strips with the corresponding primary antibody according to protein molecular weight on a shaker at 4 °C overnight. Then primary antibody recovery, the corresponding secondary antibody is incubated with the strip for one and half hours at 25 °C. TBST wash strips, then strips developed by ECL, and the results were analyzed.

2.18. Tissue transcriptome sequencing and bioinformatics analysis

Trizol reagent (Thermofisher,15596018) and 70 % ethanol were used to isolate and extract total RNA with certain purity and quality. To assess the quality of the RNA extraction was conducted using an Agilent 2100 Bioanalyzer in Hangzhou, China. The library was sequenced on the Illumina HiSeq X Ten platform to produce paired-end reads of 150 bp. Once the final transcriptome had been generated, the expression levels of all transcripts were estimated. The identification of differentially expressed mRNAs was based on the following criteria: fold change >2 or fold change <0.5 with a p-value of <0.05. Differently expressed genes (DEGs) were subjected to hierarchical clustering analyses to determine the expression patterns of the genes in different groups and samples. The analysis of DEGs was done using R software to determine gene ontology (GO) and Kyoto Encyclopedia of Genes and Genomes (KEGG) pathway enrichment.

2.19. Molecular docking

Use AutoDock Vina 1.1.2 software to perform molecular docking between Magnoflorine (PubChem CID: 73337) and protein TGFB (PDB ID: 5VQP) [19]. Perform protein pretreatment using PyMol 2.4 (remove water molecules and excess ligands, add hydrogen atoms). Chemdraw 20.0 is used to minimize the energy of compounds. AutoDock Tools 1.5.6 is used to generate PDBQT files for docking simulation. The docking box is set to encapsulate the entire protein structure. The other parameters remained at their default

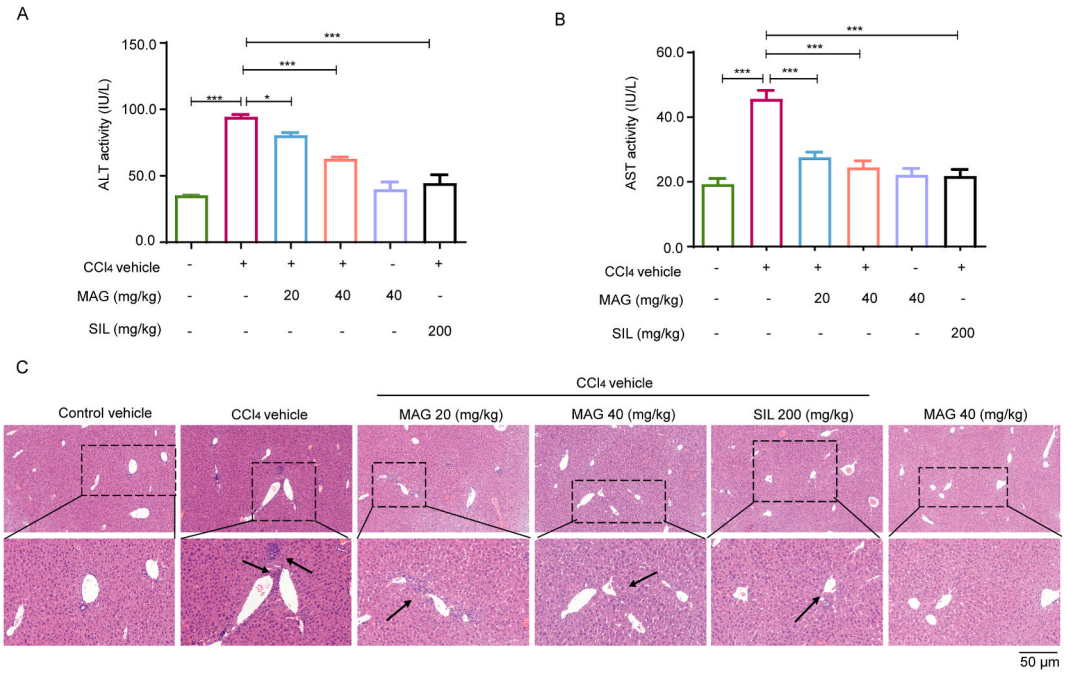

Fig. 2. Influence of MAG on ALT/AST activity and hepatic H&E stain. (A) ALT activity. (B) AST activity. (C) H&E staining. Typical images were selected for each group. (raw enlargement × 200, upper images; partial magnified image, Bottom images). Data were showed as means ± SEM (n = 3). *$P < 0.05$; ***$P < 0.001$.

values. Set the docking result to output 9 docking positions. The docking conformation with the lowest binding energy and highest clustering frequency is considered the most potential binding mode between ligands and proteins. Finally, we visualized the docking results using PLIP [20] and Pymol 2.4 software.

2.20. Statistical approach

All data are reported as mean ± SEM, and Significant differences were used by One-Way ANOVA, with the Fisher's least significant difference (LSD) post hoc test. statistically significant at $p < 0.05$.

3. Results

3.1. MAG inhibited HSC activation in vitro

A series of experiments were conducted to probe into the effect of MAG on hepatic fibrosis in vitro. To confirm whether MAG therapy could prevent HSC activation in vitro, we employed cultured HSCs. Real-time-PCR analysis indicated that the HSC-activation markers, vimentin (VIM), α-SMA (ACTA2), desmin (DES), Fibronectin 1 (FN1) and COL1A1 were downregulated following treatment with MAG (10 and 25 μM) for 48 h in a dose-dependent manner (Fig. 1B–F). Moreover, western blotting revealed that MAG (10 and 25 μM) significantly decreased VIM and α-SMA expression in activated HSCs (Fig. 1G–H).

3.2. MAG attenuated CCl_4-induced liver injury in mice

Preliminary in vitro experiments revealed that MAG reduces the expression of proteins related to liver fibrosis. Subsequently, we will establish a mouse model of liver fibrosis induced by carbon tetrachloride to investigate whether MAG can alleviate liver injury and fibrosis in vivo. The impact of MAG on serum biochemical markers, including ALT and AST, in mice with liver fibrosis induced by CCl_4 is depicted in Fig. 2A–B. The biochemical markers in the model group were significantly elevated compared to the control group,

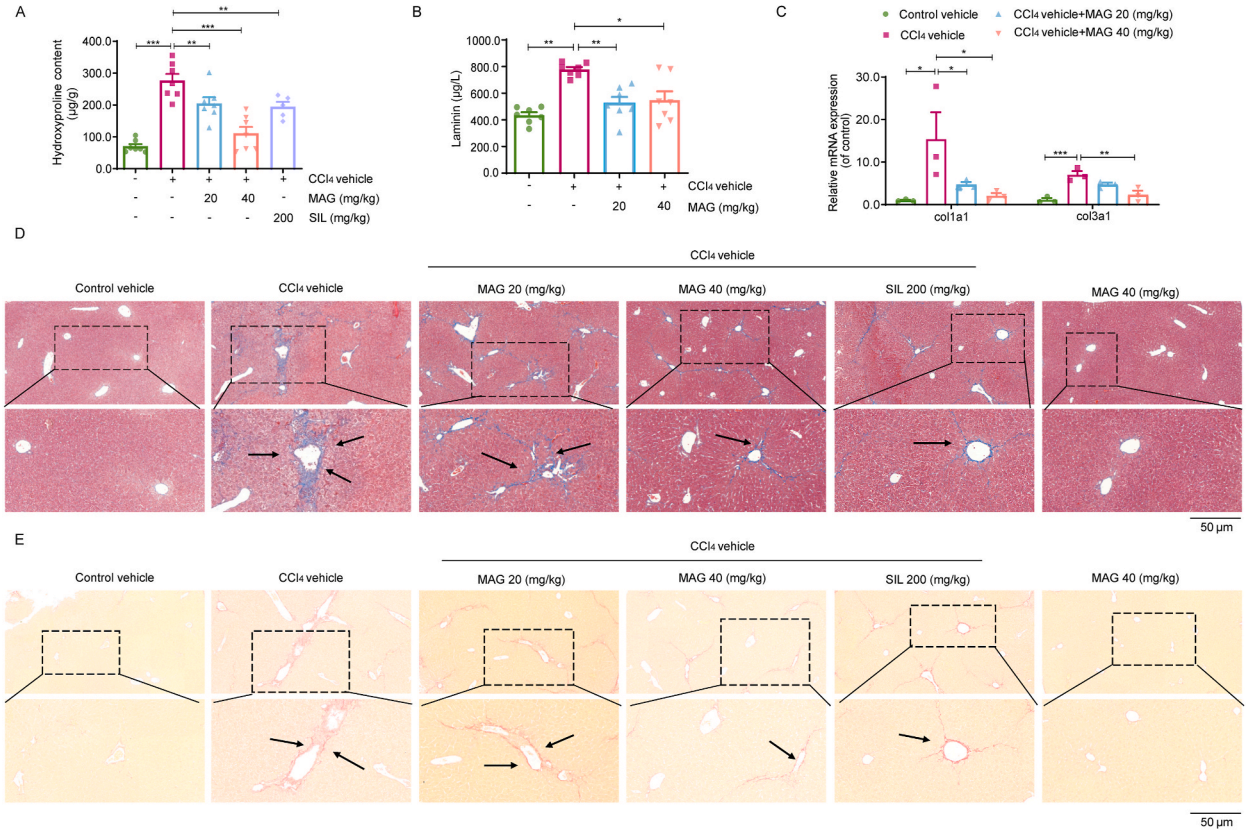

Fig. 3. The impact of MAG on liver hydroxyproline, collagen expression, and serum fibrosis indicators. (A) Hydroxyproline assay (n = 5–7). (B) Serum contents of laminin (n = 6). (C) Hepatic Col1a1and Col3a1 (n = 3). (D) Masson's trichrome stain. (E) Sirius red stain. Choose a typical picture for each group (raw magnification × 200, upper pictures; partial enlarged pictures, Bottom pictures). Data were expressed as means ± SEM. (n = 3). *$P < 0.05$; ***$P < 0.001$.

suggesting liver damage in the model group. In comparison to the model group, MAG significantly reduced ALT and AST levels, with significant differences observed at both medium and high doses ($P < 0.05$) (Fig. 2A–B). H&E staining of liver biopsy showed that MAG alleviated liver injury, hepatocyte necrosis and inflammatory cell infiltration induced by CCl_4 in mice. (Fig. 2C). SIL is an established hepatoprotective agent [21]. Notably, MAG administration (40 mg/kg) alone had no significant influence on serum AST/ALT levels and liver histomorphology in comparison with control group (Fig. 2A–C). These results suggest that MAG mitigates liver injury induced by CCl_4 in mice and does not exhibit any toxic side effects on the liver.

3.3. MAG attenuated liver fibrosis in mice induced by CCl_4

Next, we evaluated hydroxyproline content, which is the gold-standard marker for hepatic fibrosis; In the CCl_4 model group, our results indicated an increase in hydroxyproline levels in the liver tissue of mice, and MAG (20 and 40 mg/kg) and SIL (0.2 g/kg) administration significantly alleviated this increase in hydroxyproline content (Fig. 3A). We also evaluated the expression levels of COL3A1 and COL1A1, as well as serum laminin content. Treatment with CCl_4 significantly increased serum laminin levels; however, MAG administration reversed this increase (Fig. 3B). Moreover, MAG significantly decreased the CCl_4-induced increase in hepatic COL1A1 and COL3A1 mRNA expression (Fig. 3C). In addition, This study evaluated the pathological changes in mouse liver tissue using masson's trichrome staining and sirius red staining and employed a semi-quantitative collagen analysis to assess liver fibrosis. The results of the mission's trichrome staining and sirius red staining are presented in Fig. 3D–E. Normal mouse liver tissue exhibited no collagen deposition, whereas in the model group, the liver tissue was fibrotic, with collagen septa and connective tissue hyperplasia, primarily resulting in dense fibrous septa in the portal and vascular regions. Following MAG treatment, collagen deposition in the mouse liver tissue was significantly reduced compared to the control group. In contrast, treatment with MAG alone had no obvious influence on collagen sediment liver tissues in mice. (Fig. 3D–E). Collectively, these findings confirm that MAG alleviates liver fibrosis in mice induced by CCl_4.

3.4. MAG inhibited the activation of HSCs in mice treated with CCl_4

HSCs have been identified as the major matrix-producing cells during hepatic fibrosis. α-SMA, VIM, and DES are activated HSC markers [22,23]. Our data revealed that MAG (20 and 40 mg/kg) obviously decreased hepatic α-SMA, VIM, and DES mRNA and protein expression with respect to their expression levels in the CCl_4 group (Fig. 4A–E). Furthermore, hepatic α-SMA immunofluorescence staining demonstrated that MAG visibly reduced the CCl_4-induced increase in α-SMA-positive cell counts (Fig. 4F). Besides, immunohistochemical staining of hepatic vimentin demonstrated that MAG significantly reduced vimentin-positive cell counts in CCl_4-treated mice (Fig. 4G).

3.5. MAG prevented activation of HSCs by restraining TGF-β/smad pathway in vivo

The TGF-β/Smad pathway is of pivotal importance in the activation of HSCs and the generation of ECM, which leads to liver fibrosis [24]. RNA sequencing of the liver revealed a strong correlation between liver fibrosis and the collagen extracellular matrix pathway and the TGF-β signaling pathway [24], PI3K-Akt signaling pathway [25], p53 signaling pathway [26] in the Top 20 differentially expressed KEGG pathways (Fig. 4A). To verify the correlation between the aforementioned signaling pathways and our study, we employed real-time QPCR to validate key genes within the TGF-β, PI3K-Akt, and p53 signaling pathways. Our findings revealed that MAG significantly reduced the upregulation of TGF-β gene levels induced by CCl_4 (Fig. 5C), yet it exerted no significant impact on the expression of PI3K, Akt, and p53 genes (Fig. S1A). Simultaneously, to further ascertain MAG's influence on the TGF-β signaling pathway, we conducted molecular docking and discovered that the binding energy between MAG and the TGF-β protein was −6.8 kcal/mol, suggesting a strong binding affinity between MAG and the TGF-β protein (Fig. S1B). Next, the heatmap detection of the differentially expressed genes demonstrated that CCl_4-induced hepatic fibrosis was highly correlated with the Tgfb1(TGF-β) and smad3 genes (Fig. 5B). What's more, we found the suppressed effects of MAG on the TGF-β/Smad pathway in liver fibrosis in mice induced by CCl_4. RT-qPCR and WB analysis suggested that MAG (20 and 40 mg/kg) eased the increase in TGF-β mRNA and protein expression in the MAG-treated mice (Fig. 5C–E). As illustrated in Fig. 5D–F, and WB analysis revealed that the CCl_4-induced upregulation of the protein level of p-Smad was opposite following treatment with MAG (20 and 40 mg/kg).

3.6. MAG-induced ferroptosis associated with inhibition of HSCs activation

Preliminary experiments revealed that MAG can mitigate liver fibrosis by decreasing HSC marker levels. Moving forward, we will delve deeper into the specific mechanisms through which MAG alleviates liver fibrosis. Firstly, we discovered that MAG can significantly induce a dose-dependent death of HSCs through CCK-8 and FDA staining experiments (Fig. 6A–B). To further explore the mode of death of HSCs induced by MAG, we performed an RNA-sequencing analysis using mouse liver tissues from control group and CCl_4 group. It is noteworthy that the heatmap of relevant iron death genes was identified in the transcriptome sequencing of liver tissue (Fig. 6C). The results indicate that MAG may alleviate liver fibrosis by inducing ferroptosis in HSC cells. Subsequently, by measuring the levels of ferroptosis-associated biomarkers, we evaluated in vitro whether MAG mediated the activation of ferroptosis [27]. As shown in Fig. 6D–H, treatment with MAG significantly induced HSC ferroptosis, which is characterized by decreased GSH content (Fig. 6D), decreased ROS scavenging enzyme levels (Fig. 6E) and increased iron levels (Fig. 6H). Mitochondrial staining revealed that MAG (10 and 25 μM) significantly decreased mitochondrion-positive cell counts (Fig. 6F). Furthermore, Electron microscopy images of

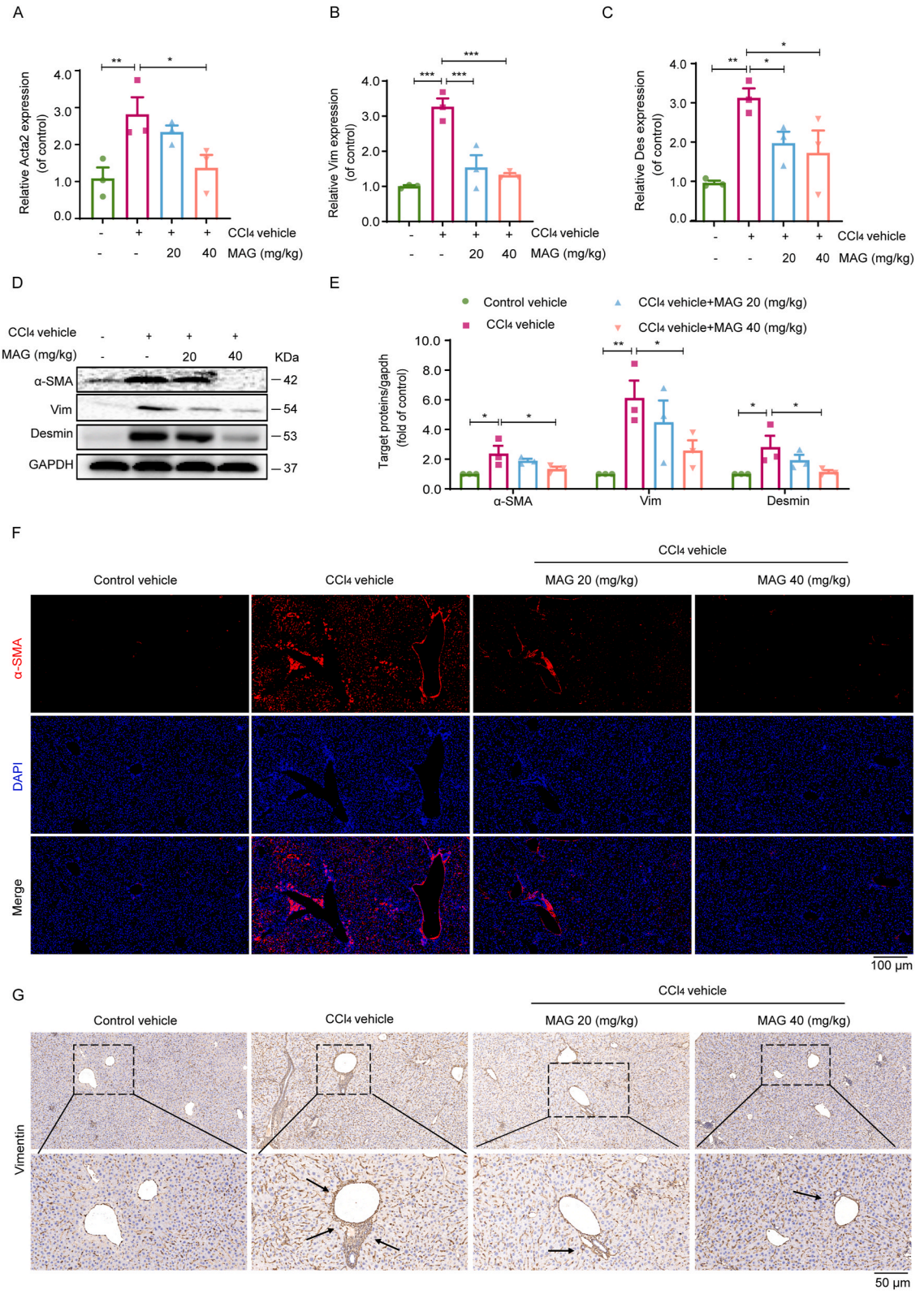

(caption on next page)

Fig. 4. The effect of MAG on the activation of HSCs in vivo. (A–C) Expression of Acta2, Vim, Des mRNA in liver (n = 3). (D) Expression of Acta2, Vim, and Des protein in the liver was detected by Western blot, and GAPDH was used as a control. (E) The Statistical result of α-SMA, Vim and Desmin. The results represent three independent experiments. (F) Liver α-SMA immunofluorescence stain (raw magnification × 100). (G) Liver Vim immunohistochemical stain. Select a typical picture for each group. Data were showed as means ± SEM. *$P < 0.05$; **$P < 0.01$; ***$P < 0.001$.

cell mitochondria confirmed the occurrence of ferroptosis. As compared to control-treated LX-2 cells, MAG-treated cells exhibited smaller, crumpled, and broken mitochondria, which are cellular morphological characteristics of ferroptosis [28] (Fig. 6G). More important, the intracellular detection of Fe^{2+} was achieved using FerroOrange. The results indicated a significant increase in Fe^{2+} within the MAG administration group when compared to the control group (Fig. 6H). GPX4, SLC7A11, and SLC40A1 are key regulators of ferroptosis [14,29,30]. We observed that MAG (10 and 25 μM) decreased GPX4, SLC40A1 and SLC7A11 protein and mRNA levels in LX-2 cells as compared to control cells (Fig. 6I–K). In conclusion, these findings revealed that MAG induced activated HSC ferroptosis in vitro.

3.7. Inhibiting ferroptosis abolishes the in vitro anti-fibrotic effects of MAG

To further elucidate the role of ferroptosis in the anti-fibrotic mechanism of MAG, the ferroptosis-specific suppressant DFO was employed to block ferroptosis [31]. The CCK-8 analyses and FDA staining revealed that LX-2 cells dealt with MAG exhibited restrained cell viability and that DFO reversed MAG-induced cell survival inhibition (Fig. 7A–B). By detecting the GSH levels in LX-2 cells, it was found that the MAG group alone significantly reduced the GSH content compared to the control group. In contrast, the simultaneous administration of DFO and MAG significantly increased the GSH content compared to the MAG group alone (Fig. 7C). In addition, when compared to the control group, the MAG treatment significantly increased ROS levels. However, co-treatment with DFO effectively antagonized this effect (Fig. 7D). Subsequently, mitochondrial staining revealed that MAG (25 μM) significantly reduced mitochondrion-positive cell counts. In contrast, DFO significantly inhibited the ferroptosis-promoting effects of MAG (Fig. 7E). Interestingly, DFO can counteract the increase in intracellular ferrous ions induced by MAG (Fig. 7F). In addition, RT-qPCR result was indicated to evaluate HSC activation and the expression levels of ferroptosis-associated biomarkers. Notably, the results of this analysis revealed that treatment with MAG markedly reduced HSC activation and the gene expression levels of ferroptosis-associated markers; DFO inhibited this effect (Fig. 7G–H). The collective findings indicated that DFO impaired the anti-fibrotic effects of MAG in vitro.

4. Discussion

These results of this study have shown that MAG significantly attenuates hepatic injury and fibrosis in mice from the CCl_4 model group. Treatment with MAG also significantly decreased the expression levels of HSC activation markers, both in vitro and in vivo, and alleviated liver fibrosis by inducing ferroptosis in HSC and reducing ECM production. Overall, the results have indicated that MAG may be clinically useful for the treatment of hepatic fibrosis. A schematic illustration of the main findings is presented in the graphic abstract.

Iron overload has long been recognized as one of the significant contributors to liver diseases. Hepatic stellate cells are rich in iron, and iron ions are an essential prerequisite for ferroptosis in these cells [13,32]. Research indicates that ferroptosis acts as a double-edged sword in the onset and progression of liver fibrosis. On the one hand, excessive iron deposition in the liver induces ferroptosis and initiates the occurrence of liver fibrosis, while ferrostatin-1 can reverse liver fibrosis. Thus, it can be inferred that iron-induced cell death, triggered by excessive iron levels in the liver in the absence of external stimuli or influences, may contribute to the progression of liver fibrosis [33,34]. On the other hand, the activation of HSCs to induce ferroptosis is emerging as a novel and promising therapeutic approach for liver fibrosis [12,13]. ZF36 (ZFP36 ring-finger protein) plays a crucial role in regulating the ferroptosis process in HSCs [12]. In animal experiments, sorafenib and other compounds induced ferroptosis in HSCs by regulating the autophagy pathway, thereby slowing down the progression of liver fibrosis. Natural products can also inhibit the occurrence and development of liver fibrosis by regulating ferroptosis. Artemisinin can elevate the levels of iron ions and reactive oxygen species (ROS) in activated HSCs, ultimately resulting in ferroptosis [35]. Additionally, magnesium glycyrrhizinate can induce ferroptosis in activated HSCs by modulating signaling pathways, including HO-1 [15]. Natural products serve as an invaluable resource in the development of therapeutic agents for treating a range of complex diseases, notably liver fibrosis. Fortunately, the natural product MAG, which we are also searching for, can induce ferroptosis in HSCs and alleviate liver fibrosis.

MAG is a novel alkaloid belonging to the Aporphine class [17]. Current studies indicate its anti-inflammatory properties, hypoglycemic effects, and its efficacy in treating central nervous system disorders, including antidepressant and anxiolytic activities [18]. MAG has been reported to possess anti-inflammatory and antioxidant properties [36,37]. MAG can also inhibit copper (Cu^{2+})-induced lipid peroxidation of both high-density lipoprotein (HDL) and low-density lipoprotein (LDL) [36]. MAG can suppress the production of nitric oxide (NO) associated with inflammation and prevent lipopolysaccharide-induced apoptosis in mouse macrophages RAW 264.7 [37]. However, whether MAG could alleviate hepatic fibrosis by inducing ferroptosis in stellate cells needs to be further investigated.

Our study demonstrates that MAG can induce the death of HSC cells. Based on this experimental result, we aim to determine the mode of death induced by MAG in HSCs. We conducted RNA-sequencing analysis and discovered that genes associated with ferroptosis were enriched. We hypothesize that MAG may induce ferroptosis in HSCs, so we further confirmed this hypothesis through ferroptosis characterization experiments. The experimental results demonstrate that MAG induces an elevation in iron ion and ROS levels in HSCs, accompanied by a decrease in GSH content. Moreover, electron microscopy and mitochondrial staining reveal that MAG leads to the

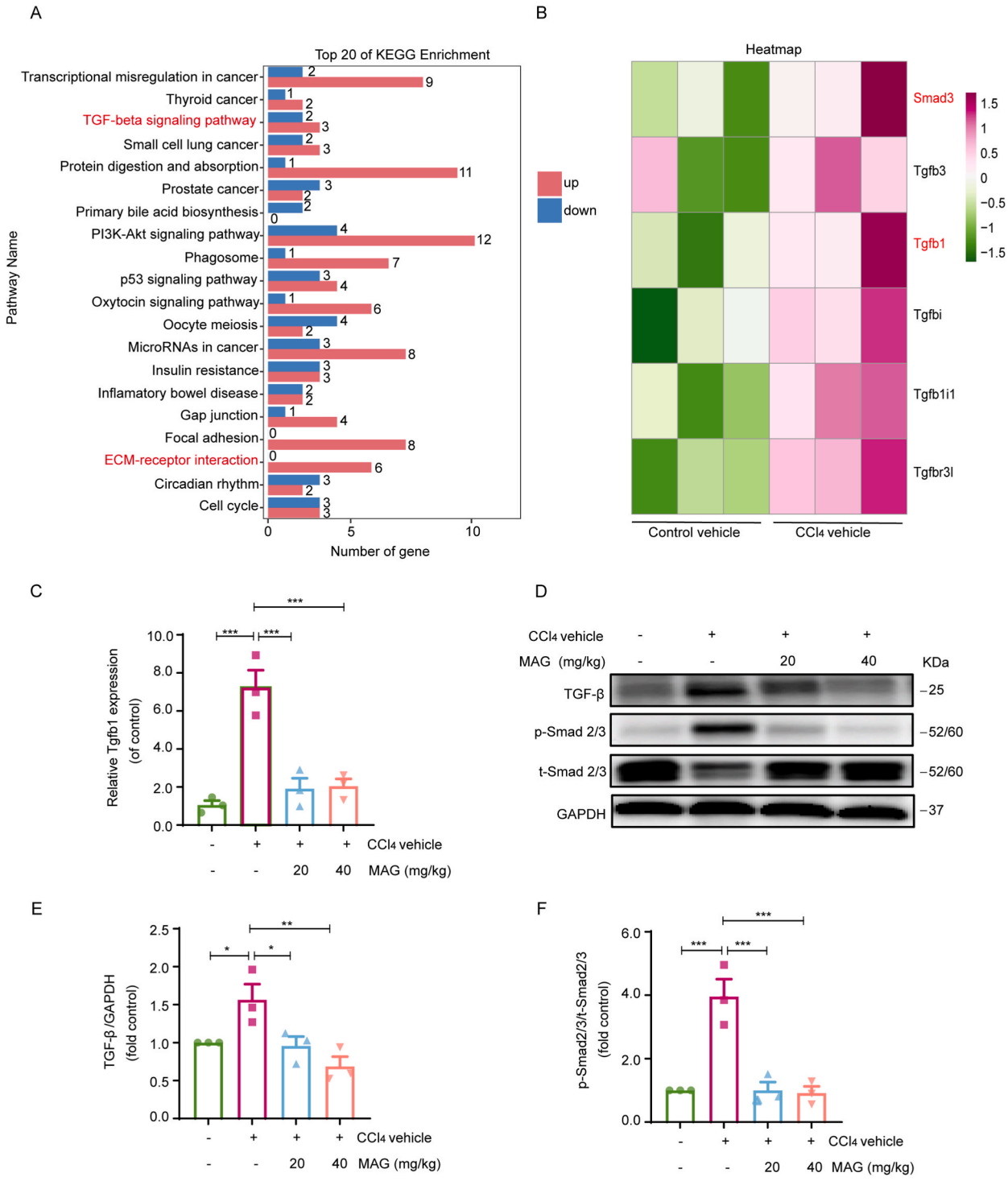

Fig. 5. MAG effects on TGF-β/Smad signal pathway in vivo. Liver tissue samples from the blank and model groups were sent for sequencing. (A) The top 20 pathways enriched by KEGG included TGF-β pathway and ECM-receptor interaction. (B) Heat map of TGF-β pathway and Smad 2/3 pathway related genes (blank control and model groups). (C) Liver Tgfb1 (TGF-β), mRNA expression (n = 3). (D) GAPDH was used as a control to detect the expression of liver TGF-β, p-Smad2/3 and t-Smad2/3 proteins by Western blot. (E) The mensurable result of TGF-β. (F) The quantified result of p-Smad2/3. The results represent three independent experiments. Data were showed as means ± SEM. $^{*}P < 0.05$; $^{**}P < 0.01$; $^{***}P < 0.001$.

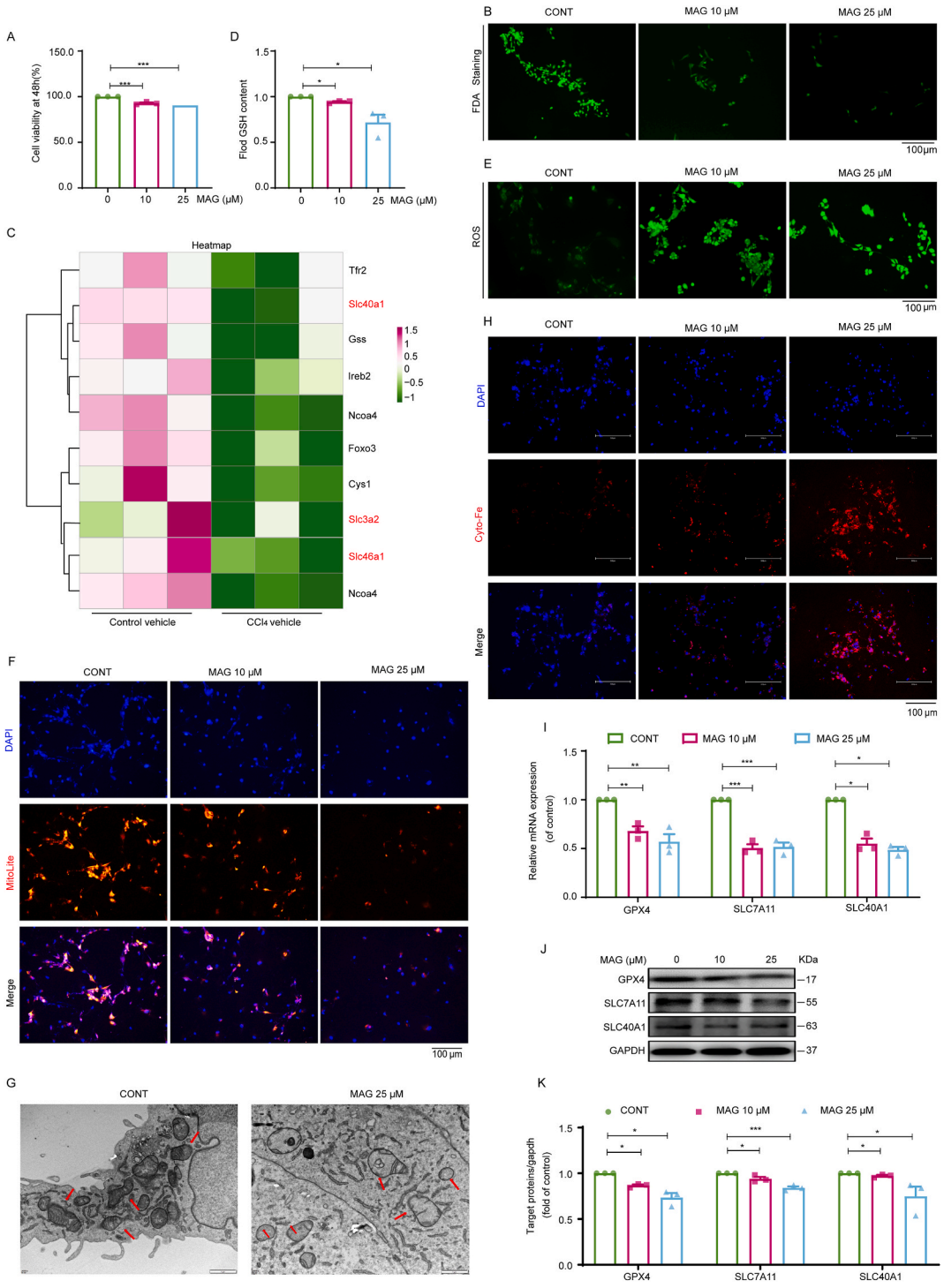

Fig. 6. MAG induces activated HSC ferroptosis in vitro. LX-2 was processed with DMSO (0.025 %, w/v) and MAG (10, 25 μM) for 48 h. (A) LX-2 cell viability was measured by CCK-8. (B) FDA staning. (C) Heat map of iron-death-related genes (control and model groups). (D) Cellular GSH amount (n = 3). (E) Cellular ROS amount evaluated Iron levels in LX-2. (F) Mitochondrial staining maps. (G) The length of mitochondria was measured and estimated by mitochondria microscopy. (H) FerroOrange (orange) stained LX2 iron and DAPI (blue) its nucleus. (I) GPX-4, SLC7A11 and SLC40A1 mRNA were expressed in LX-2 cells (n = 3). (J) GAPDH was used as a control to detect the expression of LX-2 cell GPX-4, SLC7A11, SLC40A1 proteins by Western blot. (K) The statistical result of GPX-4, SLC7A11, SLC40A1. The results represent three independent experiments. Data were represented as means ± SEM. $^{*}P < 0.05$; $^{**}P < 0.01$; $^{***}P < 0.001$.

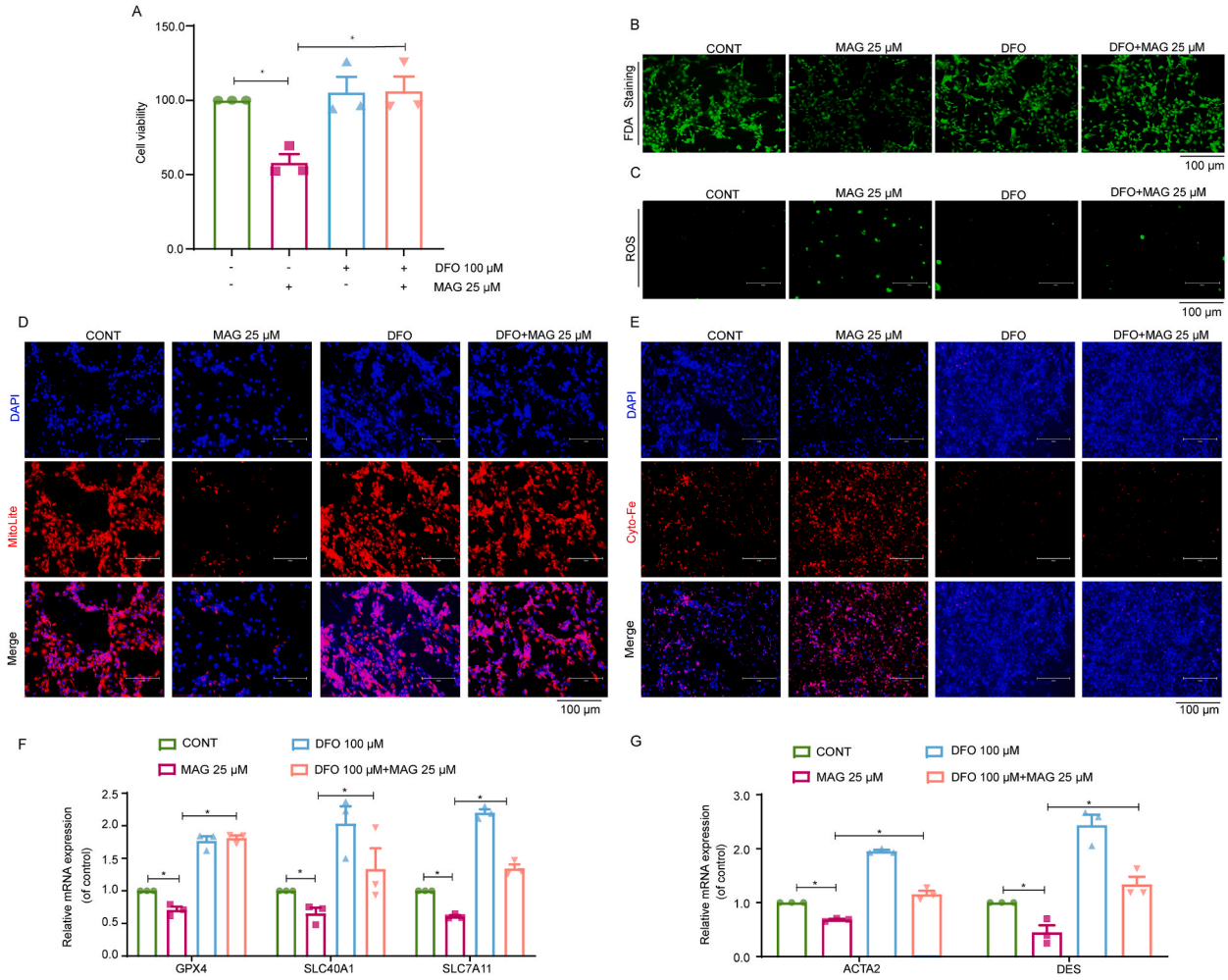

Fig. 7. Suppression of ferroptosis receded MAG-induced anti-fibrosis Influence in vitro. Activated LX-2 cells were deal with 100 μM DFO followed by 25 μM MAG treatment. (A–B) LX-2 cell viability was measured by CCK-8 and FDA staning. (C) Cellular GSH amount. (D) Cellular ROS amount. (E) Mitochondrion staining detection. (G) FerroOrange (orange). Dye the nucleus with DAPI (blue). (F) The expression of α-SMA and DES mRNA (n = 3). (H) The expression of GPX-4, SLC40A1, SLC7A11 mRNA (n = 3). The data for each panel in this figure was expressed as means ± SEM. *$P < 0.05$.

shrinkage of the cell volume and mitochondrial fragmentation in HSCs. These research outcomes preliminarily support the hypothesis that MAG induces ferroptosis in activated HSCs, which is crucial for its anti-fibrotic effects. Crucially, employing the ferroptosis-specific inhibitor DFO not only abolished the induction of ferroptosis in HSCs by MAG but also suppressed its capacity to mitigate fibrosis. These findings indicate a correlation between the alleviating effect of MAG on fibrosis and its induction of activated HSC ferroptosis.

In summary, our findings indicated for the first time that MAG-induced HSC ferroptosis could be a novel strategy for the treatment of hepatic fibrosis. These findings also indicate that MAG could serve as a novel anti-fibrotic drug in the future. However, we did not do the metabolic distribution of MAG in vivo, and this may constitute a limitation to this study. In subsequent studies, we will investigate the metabolic distribution of MAG in vivo.

CRediT authorship contribution statement

Meiling Zhang: Data curation. **Lenan Xu:** Methodology. **Chengkai Zhu:** Data curation. **Yawen Zhang:** Resources. **Ruixiang Luo:** Methodology. **Juan Ren:** Methodology. **Jie Yu:** Investigation. **Yanmei Zhang:** Formal analysis. **Guang Liang:** Writing – review & editing, Funding acquisition. **Yi Zhang:** Writing – original draft.

Ethics approval and consent to participate

All the animal experiments were performed as per the guidelines of the Experimental Animal Ethical Committee of Zhejiang Experimental Animal Center (Ethics Project Number: No. ZJCLA-IACUC-20030117).

Data availability

Data will be made available on request.

Funding

This study was supported by Zhejiang Provincial Natural Science Foundation of China under Grant No. LQ23H280021 to Y.Z., National Natural Science Foundation of China (82304840 to Y.Z.), Traditional Chinese Medicine Science and Technology Project of Zhejiang Province (2024ZF006 to Y.Z.), the General Scientific Research Project of Department of Education of Zhejiang Province (Y202045353 to Y.Z.), Basic Scientific Research Project of Hangzhou Medical College (KYYB202106 to Y.Z.), and Zhejiang Provincial Key Scientific Project (2021C03041 to G.L.).

Declaration of competing interest

The authors declare that they have no known competing financial interests or personal relationships that could have appeared to influence the work reported in this paper.

Abbreviations

MAG Magnoflorine
SIL Silymarin
DFO Deferoxamine
DMSO Dimethyl sulfoxide
HSC Hepatic stellate cell
ECM Extracellular matrix
ALT/AST Alanine/aspartate aminotransferase
GSH Glutathione
CCK-8 Cell counting kit-8
ROS Reactive oxygen species
H&E Hematoxylin-eosin
ELISA Enzyme-linked immunosorbent assay
α-SMA α-Smooth muscle actin
DES Desmin
COL1A1 collagen type I alpha 1 chain
COL3A1 collagen type III alpha 1 chain
SLC7A11 Solute carrier family-7 member-11
SLC40A1 Solute carrier family-40 member-1
Smad 2/3 SMAD family member 2/3
TGF-β Transforming growth factor-beta
VIM Vimentin
FN1 Fibronectin 1
GAPDH Glyceraldehyde-3-phosphate dehydrogenase
GPX4 Glutathione peroxidase 4
lipid peroxidation (LPO)
specific pathogen-free (SPF)
Differently expressed genes (DEGs)
gene ontology (GO)
Kyoto Encyclopedia of Genes and Genomes (KEGG)
high-density lipoprotein (HDL)
low-density lipoprotein (LDL)
nitric oxide (NO)
TRIM26 Tripartite motif-containing protein 26
PBS Phosphate buffer saline
BSA Bovine serum albumin
CCl4 carbon tetrachloride
DAB 3,3-Diaminobenzidine tetrahydrochloride

DAPI 4′, 6-Diamidino-2-phenylindole
DCFH-DA Dichlorodihydrofluorescein diacetate
DMEM Dulbecco's modified eagle medium
FDA Fluorescein diacetate
LSD Least significant difference
SEM Standard error of the mean
RT-qPCR Real-time fluorescence quantitative PCR
SDS-PAGE sodium dodecyl sulfate - polyacrylamide gel electrophoresis
PVDF polyvinylidene fluoride
TBST Tris Buffered Saline with Tween-20
ECL Enhanced chemiluminescence

Appendix A. Supplementary data

Supplementary data to this article can be found online at https://doi.org/10.1016/j.heliyon.2024.e39892.

References

[1] Y.A. Lee, M.C. Wallace, S.L. Friedman, Pathobiology of liver fibrosis: a translational success story, Gut 64 (2015) 830–841, https://doi.org/10.1136/gutjnl-2014-306842.
[2] H. Devarbhavi, S.K. Asrani, J.P. Arab, Y.A. Nartey, E. Pose, P.S. Kamath, Global burden of liver disease: 2023 update, J. Hepatol. 79 (2023) 516–537, https://doi.org/10.1016/j.jhep.2023.03.017.
[3] S.L. Friedman, Hepatic stellate cells: protean, multifunctional, and enigmatic cells of the liver, Physiol. Rev. 88 (2008) 125–172, https://doi.org/10.1152/physrev.00013.2007.
[4] J. Gao, B. Wei, T.M. de Assuncao, Z. Liu, X. Hu, S. Ibrahim, S.A. Cooper, S. Cao, V.H. Shah, E. Kostallari, Hepatic stellate cell autophagy inhibits extracellular vesicle release to attenuate liver fibrosis, J. Hepatol. 73 (2020) 1144–1154, https://doi.org/10.1016/j.jhep.2020.04.044.
[5] A. Wree, A. Eguchi, M.D. McGeough, C.A. Pena, C.D. Johnson, A. Canbay, H.M. Hoffman, A.E. Feldstein, NLRP3 inflammasome activation results in hepatocyte pyroptosis, liver inflammation, and fibrosis in mice, Hepatology (Baltimore, Md 59 (2014) 898–910, https://doi.org/10.1002/hep.26592.
[6] R.F. Schwabe, T. Luedde, Apoptosis and necroptosis in the liver: a matter of life and death, Nature reviews, Gastroenterol. Hepatol. 15 (2018) 738–752, https://doi.org/10.1038/s41575-018-0065-y.
[7] S.J. Dixon, K.M. Lemberg, M.R. Lamprecht, R. Skouta, E.M. Zaitsev, C.E. Gleason, D.N. Patel, A.J. Bauer, A.M. Cantley, W.S. Yang, B. Morrison 3rd, B. R. Stockwell, Ferroptosis: an iron-dependent form of nonapoptotic cell death, Cell 149 (2012) 1060–1072, https://doi.org/10.1016/j.cell.2012.03.042.
[8] L. Jiang, J.H. Hickman, S.J. Wang, W. Gu, Dynamic roles of p53-mediated metabolic activities in ROS-induced stress responses, Cell Cycle 14 (2015) 2881–2885, https://doi.org/10.1080/15384101.2015.1068479.
[9] M. Gao, P. Monian, N. Quadri, R. Ramasamy, X. Jiang, Glutaminolysis and transferrin regulate ferroptosis, Molecular cell 59 (2015) 298–308, https://doi.org/10.1016/j.molcel.2015.06.011.
[10] J. Chen, X. Li, C. Ge, J. Min, F. Wang, The multifaceted role of ferroptosis in liver disease, Cell Death Differ. 29 (2022) 467–480, https://doi.org/10.1038/s41418-022-00941-0.
[11] Z. Zhang, M. Guo, M. Shen, D. Kong, F. Zhang, J. Shao, S. Tan, S. Wang, A. Chen, P. Cao, S. Zheng, The BRD7-P53-SLC25A28 axis regulates ferroptosis in hepatic stellate cells, Redox Biol. 36 (2020) 101619, https://doi.org/10.1016/j.redox.2020.101619.
[12] Z. Zhang, M. Guo, Y. Li, M. Shen, D. Kong, J. Shao, H. Ding, S. Tan, A. Chen, F. Zhang, S. Zheng, RNA-binding protein ZFP36/TTP protects against ferroptosis by regulating autophagy signaling pathway in hepatic stellate cells, Autophagy 16 (2020) 1482–1505, https://doi.org/10.1080/15548627.2019.1687985.
[13] Z. Zhang, Z. Yao, L. Wang, H. Ding, J. Shao, A. Chen, F. Zhang, S. Zheng, Activation of ferritinophagy is required for the RNA-binding protein ELAVL1/HuR to regulate ferroptosis in hepatic stellate cells, Autophagy 14 (2018) 2083–2103, https://doi.org/10.1080/15548627.2018.1503146.
[14] Y. Zhu, C. Zhang, M. Huang, J. Lin, X. Fan, T. Ni, TRIM26 induces ferroptosis to inhibit hepatic stellate cell activation and mitigate liver fibrosis through mediating SLC7A11 ubiquitination, Front. Cell Dev. Biol. 9 (2021) 644901, https://doi.org/10.3389/fcell.2021.644901.
[15] M. Sui, X. Jiang, J. Chen, H. Yang, Y. Zhu, Magnesium isoglycyrrhizinate ameliorates liver fibrosis and hepatic stellate cell activation by regulating ferroptosis signaling pathway, Biomedicine & pharmacotherapy = Biomedecine & pharmacotherapie 106 (2018) 125–133, https://doi.org/10.1016/j.biopha.2018.06.060.
[16] Z. Kong, R. Liu, Y. Cheng, Artesunate alleviates liver fibrosis by regulating ferroptosis signaling pathway, Biomedicine & pharmacotherapy = Biomedecine & pharmacotherapie 109 (2019) 2043–2053, https://doi.org/10.1016/j.biopha.2018.11.030.
[17] E. Okon, W. Kukula-Koch, A. Jarzab, M. Halasa, A. Stepulak, A. Wawruszak, Advances in chemistry and bioactivity of magnoflorine and magnoflorine-containing extracts, Int. J. Mol. Sci. 21 (2020), https://doi.org/10.3390/ijms21041330.
[18] T. Xu, T. Kuang, H. Du, Q. Li, T. Feng, Y. Zhang, G. Fan, Magnoflorine: a review of its pharmacology, pharmacokinetics and toxicity, Pharmacol. Res. 152 (2020) 104632, https://doi.org/10.1016/j.phrs.2020.104632.
[19] O. Trott, A.J. Olson, AutoDock Vina: improving the speed and accuracy of docking with a new scoring function, efficient optimization, and multithreading, J. Comput. Chem. 31 (2010) 455–461, https://doi.org/10.1002/jcc.21334.
[20] M.F. Adasme, K.L. Linnemann, S.N. Bolz, F. Kaiser, S. Salentin, V.J. Haupt, M. Schroeder, Plip 2021: expanding the scope of the protein-ligand interaction profiler to DNA and RNA, Nucleic acids research 49 (2021) W530–w534, https://doi.org/10.1093/nar/gkab294.
[21] M. Abd Elmaaboud, H. Khattab, S. Shalaby, Hepatoprotective effect of linagliptin against liver fibrosis induced by carbon tetrachloride in mice, Can. J. Physiol. Pharmacol. 99 (2021) 294–302, https://doi.org/10.1139/cjpp-2020-0049.
[22] S.N. Greenhalgh, K.P. Conroy, N.C. Henderson, Cre-ativity in the liver: transgenic approaches to targeting hepatic nonparenchymal cells, Hepatology (Baltimore, Md 61 (2015) 2091–2099, https://doi.org/10.1002/hep.27606.
[23] J.E. Puche, Y. Saiman, S.L. Friedman, Hepatic stellate cells and liver fibrosis, Compr. Physiol. 3 (2013) 1473–1492, https://doi.org/10.1002/cphy.c120035.
[24] C. Yang, M. Zeisberg, B. Mosterman, A. Sudhakar, U. Yerramalla, K. Holthaus, L. Xu, F. Eng, N. Afdhal, R. Kalluri, Liver fibrosis: insights into migration of hepatic stellate cells in response to extracellular matrix and growth factors, Gastroenterology 124 (2003) 147–159, https://doi.org/10.1053/gast.2003.50012.
[25] E. Shamsan, M. Almezgagi, M. Gamah, N. Khan, A. Qasem, L. Chuanchuan, F. Haining, The role of PI3k/AKT signaling pathway in attenuating liver fibrosis: a comprehensive review, Front. Med. 11 (2024) 1389329, https://doi.org/10.3389/fmed.2024.1389329.
[26] S. Yu, G. Ji, L. Zhang, The role of p53 in liver fibrosis, Front. Pharmacol. 13 (2022) 1057829, https://doi.org/10.3389/fphar.2022.1057829.
[27] T. Hirschhorn, B.R. Stockwell, The development of the concept of ferroptosis, Free radical biology & medicine 133 (2019) 130–143, https://doi.org/10.1016/j.freeradbiomed.2018.09.043.
[28] J.Y. Cao, S.J. Dixon, Mechanisms of ferroptosis, Cell. Mol. Life Sci. : CMLS 73 (2016) 2195–2209, https://doi.org/10.1007/s00018-016-2194-1.

[29] X. Chen, J. Li, R. Kang, D.J. Klionsky, D. Tang, Ferroptosis: machinery and regulation, Autophagy 17 (2021) 2054–2081, https://doi.org/10.1080/15548627.2020.1810918.
[30] F. Ursini, M. Maiorino, Lipid peroxidation and ferroptosis: the role of GSH and GPx4, Free radical biology & medicine 152 (2020) 175–185, https://doi.org/10.1016/j.freeradbiomed.2020.02.027.
[31] H. Wang, P. An, E. Xie, Q. Wu, X. Fang, H. Gao, Z. Zhang, Y. Li, X. Wang, J. Zhang, G. Li, L. Yang, W. Liu, J. Min, F. Wang, Characterization of ferroptosis in murine models of hemochromatosis, Hepatology (Baltimore, Md 66 (2017) 449–465, https://doi.org/10.1002/hep.29117.
[32] E.R. Anderson, Y.M. Shah, Iron homeostasis in the liver, Compr. Physiol. 3 (2013) 315–330, https://doi.org/10.1002/cphy.c120016.
[33] Y. Yu, L. Jiang, H. Wang, Z. Shen, Q. Cheng, P. Zhang, J. Wang, Q. Wu, X. Fang, L. Duan, S. Wang, K. Wang, P. An, T. Shao, R.T. Chung, S. Zheng, J. Min, F. Wang, Hepatic transferrin plays a role in systemic iron homeostasis and liver ferroptosis, Blood 136 (2020) 726–739, https://doi.org/10.1182/blood.2019002907.
[34] M. Aldrovandi, M. Conrad, Ferroptosis: the good, the bad and the ugly, Cell Res. 30 (2020) 1061–1062, https://doi.org/10.1038/s41422-020-00434-0.
[35] L. Wang, Z. Zhang, M. Li, F. Wang, Y. Jia, F. Zhang, J. Shao, A. Chen, S. Zheng, P53-dependent induction of ferroptosis is required for artemether to alleviate carbon tetrachloride-induced liver fibrosis and hepatic stellate cell activation, IUBMB Life 71 (2019) 45–56, https://doi.org/10.1002/iub.1895.
[36] T.M. Hung, J.P. Lee, B.S. Min, J.S. Choi, M. Na, X. Zhang, T.M. Ngoc, I. Lee, K. Bae, Magnoflorine from Coptidis Rhizoma protects high density lipoprotein during oxidant stress, Biological & pharmaceutical bulletin 30 (2007) 1157–1160, https://doi.org/10.1248/bpb.30.1157.
[37] S. Guo, K. Jiang, H. Wu, C. Yang, Y. Yang, J. Yang, G. Zhao, G. Deng, Magnoflorine ameliorates lipopolysaccharide-induced acute lung injury via suppressing NF-κB and MAPK activation, Front. Pharmacol. 9 (2018) 982, https://doi.org/10.3389/fphar.2018.00982.